Atmos. Chem. Phys. Discuss., 15, 9203–9252, 2015
www.atmos-chem-phys-discuss.net/15/9203/2015/
doi:10.5194/acpd-15-9203-2015

Atmospheric Chemistry and Physics Discussions

Springtime variability of lower tropospheric ozone over Eastern Asia: contributions of cyclonic activity and pollution as observed from space with IASI

G. Dufour[1], M. Eremenko[1], J. Cuesta[1], C. Doche[2], G. Foret[1], M. Beekmann[1], A. Cheiney[3,1], Y. Wang[4], Z. Cai[4], Y. Liu[4], M. Takigawa[5], Y. Kanaya[5], and J.-M. Flaud[1]

[1]Laboratoire Inter-universitaire des Systèmes Atmosphériques (LISA), UMR7583, Universités Paris-Est Créteil et Paris Diderot, CNRS, Créteil, France
[2]Météo France, Direction Inter-Régionale Sud-Ouest, Division Etudes et Climatologie, Mérignac, France
[3]Institut National de l'Environnement industriel et des RISques, INERIS, Verneuil-en-Halatte, France
[4]Key Laboratory of middle Atmosphere and Global Environment Observation, Institute of Atmospheric Physics, Chinese Academy of Sciences, Beijing, China
[5]Japan Agency for Marine-Earth Science and Technology, Yokohama, Japan

Received: 18 February 2015 – Accepted: 13 March 2015 – Published: 27 March 2015

Correspondence to: G. Dufour (gaelle.dufour@lisa.u-pec.fr)

Published by Copernicus Publications on behalf of the European Geosciences Union.

ACPD
15, 9203–9252, 2015

Abstract

We use satellite observations from IASI (Infrared Atmospheric Sounding Interferometer) on board the MetOp-A satellite to evaluate the springtime daily variability of lower tropospheric ozone at the scale of Eastern Asia. Lower tropospheric partial columns from surface to 6 km are retrieved from IASI with a maximum of sensitivity between 3 and 4 km. We focus our analysis on the month of May 2008 for which tropospheric ozone presents typically amongst the largest concentrations along the year. We combine IASI observations with meteorological reanalyses from ERA-Interim in order to investigate the processes that control the spatial and temporal distribution of lower tropospheric ozone, especially in case of ozone enhancement. The succession of low- and high-pressure systems drives the day-to-day variability of lower tropospheric ozone over North East Asia. The analysis of two episodes with ozone enhancement at the synoptic scale of East Asia shows that the reversible subsiding and ascending ozone transfers in the UTLS region occurring in the vicinity of low-pressure systems and related to tropopause height affect the upper and lower tropospheric ozone over large regions, especially north to 40° N and largely explain the ozone enhancement observed with IASI for these latitudes. Irreversible downward transport of ozone-rich air masses from the UTLS to the lower troposphere occurs more locally. Its contribution to the lower tropospheric ozone column is difficult to dissociate from the tropopause perturbations induced by the weather systems. For regions south to 40° N, a significant correlation between lower tropospheric ozone and carbon monoxide (CO) observations from IASI has been found, especially over North China Plain (NCP). Considering carbon monoxide observations as pollutant tracer, the O_3-CO correlation indicates that the photochemical production of ozone from primary pollutants emitted over such large polluted regions significantly contributes to the ozone enhancements observed with IASI in the lower troposphere. When low-pressure systems circulate over NCP, stratospheric and pollution sources play a concomitant role in the ozone enhancements. Moreover, in that case, evidence of pollutant export from NCP towards the east is shown. Finally, we

ACPD
15, 9203–9252, 2015

show that semi-independent columns of ozone from the surface up to 12 km associated with CO columns from IASI constitute a powerful observational dataset to investigate the processes controlling tropospheric enhancement of ozone at synoptic scales.

1 Introduction

In addition to be an important greenhouse gas (Stevenson et al., 2013), tropospheric ozone (O_3) plays a central role in atmospheric chemistry and air quality, by controlling the oxidation processes through the formation of hydroxyl radicals (OH) (Monks, 2005; Monks et al., 2014). Ozone at high concentrations near the surface is a pernicious pollutant harmful to both human health and vegetation (Seinfeld and Pandis, 1997; World Health Organization, 2013). Enhancements of ozone in the mid and lower troposphere result from photochemical production from precursors (NOx and hydrocarbons) and from stratosphere–troposphere exchanges (STE) (Lelieveld and Dentener, 2000). The relative contribution of these sources depends on the season. It is well established that the peak activity of STE occurs during winter and spring (Monks, 2000) whereas the photochemical production is more active during summer period. The crucial role of weather systems (cyclonic activity) in determining the tropospheric ozone variability has been well established (e.g. Carmichael et al., 1998; Cooper et al., 1998, 2002a; Ding et al., 2009). These weather systems are associated with tropopause perturbation, especially low tropopauses, and then with subsiding and ascending ozone transfer in the upper troposphere–lower stratosphere (UTLS) region. In addition, irreversible transfers of ozone can be expected such as stratosphere–troposphere exchanges that would take place preferentially in the western and southern flank of the trough (e.g. Ancellet et al., 1994; Holton et al., 1995; Liu et al., 2013), and downward transport from the UTLS to the lower troposphere (e.g. Cooper et al., 2002a). Conceptual models have been proposed to describe airstreams related to traveling low-pressure systems at the midlatitudes (e.g. Cooper et al., 2002b). Two main mechanisms are responsible for part of the ozone temporal and spatial variations observed in the troposphere. The

ACPD
15, 9203–9252, 2015

dry airstream (DA) occurring behind cold fronts is responsible for a strong downward transport of ozone from the ULTS down to the middle troposphere. It is often linked to tropopause folding. This downward transport can affect ozone concentrations down to the surface, especially at high altitudes sites (e.g. Carmichael et al., 1998; Stuepbach et al., 1999; Dempsey, 2014). On the contrary, warm conveyor belts (WCB) occurring before the cold front allow the transport of air masses and then pollutants from the planetary boundary layer to the free troposphere (e.g. Bethan et al., 1998; Hannan et al., 2003; Cooper et al., 2004; Ding et al., 2009; Foret et al., 2014). The WCBs associated with frontal activity have been studied mainly under the scope of their role in the long-range transport of pollutants, because they lift pollutants to levels where horizontal transport is more efficient. Several studies focusing on the trans-Pacific transport of pollutants from East Asia towards the United States have shown the importance of the frontal systems in this transport during springtime using both model simulations (e.g. Bey et al., 2001; Liu et al., 2003; Mari et al., 2004; Lin et al., 2010) and dedicated field campaigns (e.g. Jaffe et al., 1999; Cooper et al., 2004; Liang et al., 2004; Oshima et al., 2004).

Since the past decades, East Asia and in particular China have been experiencing a rapid economic growth. The related increasing anthropogenic emissions of pollutants (Richter et al., 2005; Lin et al., 2013) lead to regional ozone concentrations amongst the highest in the world (e.g. Chan and Yao, 2008; Zhao et al., 2009; Lelieveld and Dentener, 2000; Wang et al., 2012; Safieddine et al., 2013). Due to the rapidly changing emissions in China, the respective contribution of anthropogenic and natural perturbation to tropospheric ozone in China and its variability constitutes a crucial issue to document and better understand. The seasonal variations of ozone in East Asia and especially the role of the summer Asian monsoon leading to a summer minimum have been extensively studied from model simulations (e.g. Mauzerall et al., 2000; Yamaji et al., 2006; Li et al., 2007), in situ (e.g. Ding et al., 2008; Wang et al., 2009) and satellite (e.g. Dufour et al., 2010) observations. However, at the synoptic scale, the direct impact of the weather systems on the tropospheric ozone distribution above China and its

ACPD
15, 9203–9252, 2015

daily variability has been less extensively considered or, if so, mainly under the scope of the long-range transport of pollutants and export to the Pacific Ocean. A recent study investigates the dynamical and chemical features induced in the upper troposphere by cut-off lows over northeast China using limb and nadir satellite sounders (Liu et al., 2013).

The progress made in satellite observations of tropospheric ozone during the last decade (e.g. Worden et al., 2007; Eremenko et al., 2008; Liu et al., 2010; Nakatani et al., 2012) offers a new opportunity to evaluate ozone distribution and its daily variability including the role of transport at the synoptic scale (e.g. Doche et al., 2014). The satellite provides an unprecedented spatial coverage that allows new insight into how synoptic processes impact ozone distributions. The first satellite measurements of tropospheric ozone were obtained using ultraviolet-visible (UV) sounders (e.g. Fishmann et al., 2003; Liu et al., 2007). Later on, the development of thermal infrared nadir sounders allowed accurate measurements of partial tropospheric ozone columns (Coheur et al., 2005; Worden et al., 2007; Dufour et al., 2012; Safieddine et al., 2013). Using GOME and OMI UV sounders, Nakatani et al. (2012) show a persistent belt of enhanced tropospheric columns of ozone at mid-latitudes over East Asia throughout the year partly attributed to stratospheric intrusion near the subtropical jet. The tropospheric contribution to the enhanced ozone column has been assessed using model simulations. Nakatani et al. (2012) underlined the difficulty differentiating the stratospheric and tropospheric origins of ozone in the tropospheric columns observed by satellite. This difficulty was already stated by de Laat et al. (2005). However, it has been demonstrated that thermal infrared sounders like IASI on board MetOp (Clerbaux et al., 2009) allow the retrieval of semi-independent partial columns of ozone within the troposphere (Eremenko et al., 2008; Dufour et al., 2010, 2012; Saffiedine et al., 2013; Barret et al., 2011). Dufour et al. (2010) show the ability of IASI to provide independent information on the seasonal variability of lower and upper tropospheric ozone over Eastern Asia. On shorter-term periods of the order of several days, the retrieved ozone profile with IASI allows the identification of the origin of the observed tropospheric ozone in

ACPD
15, 9203–9252, 2015

specific cases. Very recently, Hayashida et al. (2015) show ozone enhancement in the lower troposphere over East Asia using the OMI space-borne ultraviolet spectrometer. They attribute the enhancement mainly to the emissions of ozone precursors from open crop residue burning after the winter wheat harvest.

In this paper, we use the IASI observation of lower tropospheric ozone to investigate the influence of synoptic scale weather systems on the distribution of ozone over East Asia. We focus our study on the month of May 2008 for which tropospheric ozone presents typically amongst the largest concentrations along the year. Two cases studies associated with travelling low-pressure systems and presenting enhanced ozone in the lower troposphere are analysed. In the two cases, the contributions of the descending air from the UTLS in the vicinity of the weather systems and of the photochemical production of ozone are investigated based on IASI observations of ozone (O_3) and carbon monoxide (CO) as well as on meteorological indicators. Through these two case studies, we demonstrate that semi-independent ozone columns between the surface and 12 km from IASI associated with simultaneous CO measurements provide a powerful observational dataset to identify, at least partly, the stratospheric and anthropogenic origin of lower free tropospheric ozone. The domain considered in the study as well as some geographical information are given in Fig. 1.

The paper is structured as follow. In Sect. 2, the different satellite and meteorological datasets are described. As a new version of the IASI ozone product is used for this study, we provide a summary of the validation of the product with a specific focus on East Asia. In Sects. 4 and 5, the two case studies are presented in details. A general discussion is given in Sect. 6 as well as a conclusion in Sect. 7.

ACPD
15, 9203–9252, 2015

2 Datasets description

2.1 The IASI instrument

The IASI (Infrared Atmospheric Sounding Interferometer) (Clerbaux et al., 2009) instrument, on board the MetOp-A platform since Octobre 2006, is a nadir-viewing Fourier transform spectrometer. It operates in the thermal infrared between 645 and 2760 cm^{-1} with an apodized resolution of 0.5 cm^{-1}. The field of view of the instrument is composed of a 2 × 2 matrix of pixels with a diameter at nadir of 12 km each. IASI scans the atmosphere with a swath width of 2200 km and crosses the equator at two fixed local solar times 9.30 a.m. (descending mode) and 9.30 p.m. (ascending mode), allowing the monitoring of atmospheric composition twice a day at any location. The large spectral coverage, the high radiometric sensitivity and accuracy, and the rather high spectral resolution of the instrument allow this instrument to measure the global distribution of several important atmospheric species (e.g. Boynard et al., 2009; George et al., 2009; Clarisse et al., 2011).

2.2 Lower tropospheric ozone from IASI

The IASI ozone profiles and partial columns considered in this paper are retrieved using the method described in Eremenko et al. (2008). The retrieval is performed using the radiative transfer model KOPRA (Karlsruhe Optimised and Precise Radiative transfer Algorithm) and its inversion module KOPRAFIT (Stiller et al., 2000; Höpfner et al., 2000), both adapted to the nadir-viewing geometry. A constrained least squares fit method with an analytical altitude-dependent regularization is used (Kulawik et al., 2006). The applied regularization method is detailed in Eremenko et al. (2008). To summarize, the regularization matrix is a combination of first order Tikhonov constraints (Tikhonov, 1963) with altitude-dependent coefficients. The coefficients are optimized both to maximize the degrees of freedom (DOF) of the retrieval and to minimize the total error on the retrieved profile. Compared to previous studies using this algorithm

ACPD
15, 9203–9252, 2015

(Eremenko et al., 2008; Dufour et al., 2010, 2012), several changes have been made. The emissivity of the surface is now taken into account based on a global monthly IASI-derived climatology (Zhou et al., 2011) allowing a better retrieval above arid regions. Different a priori and constraints are used depending on the tropopause height. This new scheme was introduced to reduce possible compensation effects during the retrieval procedure. An automatic detection of the tropopause height (calculated from the temperature profile retrieved from IASI using the definition based on the lapse rate criterion (WMO, 1957)) has been introduced to discriminate between polar, midlatitudes, and tropical situations. If the tropopause is lower than 10 km, polar constraint and a priori profile are used. If tropopause is between 10 and 14 km, midlatitude constraint and a priori profile are used. If tropopause is higher than 14 km, tropical constraint and a priori are used. The midlatitude and tropical regularization matrices are those already used in Eremenko et al. (2008) and Dufour et al. (2010, 2012) respectively. The polar constraint has been specifically developed following the same method than in Eremenko et al. (2008). The a priori profiles are compiled from the ozonesonde climatology of McPeters et al. (2007). The midlatitude a priori profile is set to the climatological profile of the 30–60° N latitude band for summer. The tropical a priori profile is set to the climatological profile of the 10–30° N latitude band over the year. The polar profile is set to the climatological profile of the 60–90° N latitude band for summer. As the version of the ozone product used in this study significantly differ from the version extensively validated in Dufour et al. (2012), a new validation against ozonesondes has been conducted and the results are presented in Sect. 3. The modifications of the algorithm do not influence the vertical sensitivity of IASI. As shown in Dufour et al. (2010, 2012), two semi-independent partial columns of ozone between the surface and 12 km can be considered: the lower tropospheric column integrating the ozone profile from the surface to 6 km altitude – above sea level (a.s.l.) – and the upper tropospheric column integrating the ozone profile from 6 to 12 km altitude. Note that the latter column can include stratospheric air masses depending on the tropopause height. The averaging kernels give information on the vertical sensitivity and resolution of the retrieval.

ACPD
15, 9203–9252, 2015

The lower tropospheric column shows a maximum of sensitivity typically between 3 and 4 km with a limited sensitivity to the surface (Dufour et al., 2012). This implies that the ozone concentration profile in the lower troposphere is preferentially incremented at these altitudes during the retrieval process, independently if the true ozone profile is perturbed at other altitudes, especially at the surface. Moreover, it is worth noting that the partial columns are only semi-independent. It means that they may include partial information from altitudes outside their altitude range. For example, the lower tropospheric column includes information from altitudes higher than its upper limit (6 km). In order to estimate the fraction of contamination by higher altitudes of the lower tropospheric column, we calculated the ratio between the integral of the averaging kernel of the lower tropospheric column from 6 to 60 km and the integral from the surface to 60 km. Higher atmospheric layers contribute to about 20 to 30 % of the lower tropospheric column in the midlatitude air masses (not shown). Note that only the morning overpasses of IASI are considered for this study in order to remain in thermal conditions with a better sensitivity to the lower troposphere.

2.3 Carbon monoxide from IASI

The CO data used here are retrieved from the IASI spectra within the 2143–2181.25 cm^{-1} spectral range using the FORLI-CO retrieval code from the Université Libre de Bruxelles (ULB). FORLI-CO retrievals give CO concentration profiles using the optimal estimation method (Rodgers, 2000) and a single a priori profile. More details are given in Hurtmans et al. (2012). The IASI FORLI-CO product used in this study is the total column, publicly available from the Ether website (http://www.pole-ether.fr). Note that only half of the pixels are available for the year 2008. This explains the difference in measurement density between O_3 and CO observations in the different figures. Carbon monoxide is often used as an indicator of biomass burning and anthropogenic pollution (e.g. Edwards et al., 2004; McMillan et al., 2010). In this study, we use the IASI CO columns as an anthropogenic pollution tracer.

ACPD
15, 9203–9252, 2015

2.4 Meteorological dataset

Meteorological data from the ECMWF ERA-Interim reanalysis are used in our analyses. The reanalysis is based on a 4D-Var assimilation system with a 12 h analysis window. The spatial resolution of the data set is approximately 80 km on 60 vertical levels from the surface up to 0.1 hPa (Dee et al., 2011). In our analyses, the meteorological parameters are taken at 00:00 UTC, corresponding roughly to the morning overpass time of IASI. The main variables considered in this study are the geopotential height, the potential vorticity (PV), and the horizontal wind field (u and v components) as well as the equivalent potential temperature, the vertical velocity and the convective available potential energy. The geopotential height associated with the horizontal wind at 850 hPa give a proxy for describing the weather situation and the horizontal transport in the lower troposphere, whereas the same parameters at 300 hPa describe the situation in the UTLS. We also calculate the equivalent potential temperature at 850 and 300 hPa from temperature, relative humidity and specific humidity fields (Bolton, 1980) as an indicator of air masses origin (Holton, 2004). Potential vorticity (PV) is often used as a tracer of tropopause height and of air masses origin (e.g. Bethan et al., 1996). PV values between 1 and 1.6 PVU are representative of the upper troposphere whereas PV values larger than 1.6 PVU are indicators of air mass origin above the dynamical tropopause. In this study, we consider mainly the PV averaged between 300 and 500 hPa with a 50 hPa interval as we are mainly interested by the impact of stratospheric air masses to the free troposphere. In order to investigate the ascending motion of air masses, especially from the boundary layer towards the free troposphere within weather systems, we examine the vertical velocity at different pressure levels as well as the convective available potential energy (CAPE), which informs on the capability of the low-pressure system to vertically transport air masses by convection.

ACPD
15, 9203–9252, 2015

3 Validation of IASI lower tropospheric ozone

Significant changes in the ozone retrieval procedure compared to the validation exercise reported in Dufour et al. (2012) have been made as described in Sect. 2.2. A new validation exercise was done to evaluate the new version of the ozone product. We use a database of ozonesonde measurements from 2007 to 2012 including 27 stations in the midlatitudinal band (30–60°) in both hemispheres and 16 stations in the tropical band (30° S–30° N). The list of the stations and the relative information are provided in Table 1. The coincidence criteria used for the validation are 1° around the station, a time difference smaller than 6 h and a minimum of 10 clear-sky pixels matching these criteria. The results of the comparison between IASI ozone retrievals and ozonesonde measurements are summarized in Table 2 for different partial columns. Bias in the lower tropospheric column (surface to 6 km a.s.l.) is small −0.6 DU (−2.8 %) and comparable to the bias estimated at the midlatitudes with the previous version of the product (Dufour et al., 2012). The error estimated is about 2.8 DU (14 %) with a correlation coefficient of 0.70. A validation exercise considering East Asian ozonesonde stations only (Beijing, Hong Kong, Naha, Sapporo and Tateno) indicates a larger bias in the lower troposphere with IASI underestimating ozone partial columns by about 2 DU (9 %). However, the time coincidence criterion had to be relaxed to 24 h to allow a more significant number of coincidences between IASI observations and ozonesonde measurements. The larger time difference between IASI and ozonesonde osbervations may partly explain the larger bias in this case.

4 Case study of 4–6 May 2008: influence of weather systems on tropospheric ozone distribution

An episode of high ozone is observed in the lower troposphere with IASI in North East Asia from 4 to 6 May 2008. This episode is associated with a low-pressure system travelling from Mongolia through North China to the extreme north of Japan. In this

ACPD
15, 9203–9252, 2015

section, we investigate which processes contribute to the ozone enhancement. Figure 2 describes the meteorological situation for this period. Figure 3 shows the lower and upper tropospheric ozone columns observed with IASI as well as the total CO columns, also observed with IASI, and the PV averaged between 300 and 500 hPa, taken at the coordinates of IASI pixels.

4.1 Influence of the low-pressure system on the tropospheric ozone distribution

On 4 May 2008, a large cold front associated to the low-pressure system extends from Mongolia to South China (blue line in Fig. 2a). The region over Mongolia behind the cold front and north to the polar jet situated around 40° N that day (Fig. 2d) is strongly influenced by polar air masses, characterized by a tropopause height smaller than 9 km (Fig. 2g). In the same region, PV values larger than 1.6 PVU are observed, indicating that the upper troposphere is under the influence of lower stratospheric air masses (Fig. 3j). The spatial correlation of low tropopauses and large PV values reveals that the upper troposphere is mainly affected by reversible subsiding ozone transfer in this case. Upper tropospheric ozone columns (from 6 to 12 km) larger than 40 DU are observed with IASI in the same region (Fig. 3g). The good spatial correlation of these columns with both large PV values and low tropopause height suggests that the upper tropospheric columns of ozone from IASI can be used as a proxy to identify regions of enhanced tropospheric ozone associated with low tropopause inside troughs and possibly due to downward transport from the stratosphere. Large lower tropospheric ozone columns (surface to 6 km a.s.l.) are also retrieved from IASI for the same region of large PV (Fig. 3a). The low tropopause height in these regions induces an enhancement of ozone in the upper and free troposphere that may partly explain the enhanced lower tropospheric columns observed with IASI. Moreover, as discussed in Sect. 2.2, the lower tropospheric column is partly contaminated by ozone from higher altitudes. As the tropopause is low in this region, the atmospheric layers contaminating the lower tropospheric column present lower stratospheric concentrations of ozone and may lead to

ACPD
15, 9203–9252, 2015

an overestimation of the lower tropospheric columns. However, it is difficult to estimate the overestimation in this case because no ozonesonde observations were available in the region.

On 5 May 2008, the low-pressure system moves to the East with the associated cold front extending from North China to the Southern Japanese Islands (Fig. 2b). Polar air masses with low tropopauses influence the troposphere north to Korea for latitudes higher than 37° N (Fig. 2e and h). Upper tropospheric ozone columns larger than 40 DU (Fig. 3h) as well as lower tropospheric columns larger than 28 DU (Fig. 3b) are observed with IASI in this region. The good spatial correlation between the ozone partial columns and the PV values larger than 1.6 PVU (Fig. 3k) and the tropopause heights lower than 9 km (Fig. 2h) suggest that reversible subsiding ozone transfer contributes for a large part of the tropospheric ozone enhancement observed that day. The analysis of the PV for different pressure levels shows that a small area on the east coast of Korea, sampled with IASI and showing enhanced lower tropospheric ozone, presents PV values larger than 1 PVU down to 600 hPa (Fig. 4a). This suggests that the lower tropospheric column is affected by the downward transport of upper tropospheric air, rich in ozone, within the dry airstream occurring behind the cold front. In the case presented here (Fig. 3b), the downward transport seems more effective in the southeast flank of the low-pressure system. The contribution of the downward transport on lower tropospheric ozone is difficult to assess more precisely from IASI observations due to the limited vertical resolution.

On 6 May 2006, the low-pressure system is located to the North of Japan (Fig. 2c). A similar influence of polar air masses with low tropopauses compared to the two previous days is noticed behind the cold front (Fig. 2f and j). This influence is characterized by large lower and upper tropospheric ozone columns (Fig. 3c and i, resp.) as well as PV values larger than 1.6 PVU (Fig. 3l). As for 5 May 2008, the analysis of PV for different pressure levels shows a well-defined area in the northeast of Tokyo with PV values larger than 1 PVU at 600 hPa (Fig. 4b). This region is situated to the southeast flank of the weather system and lower tropospheric ozone columns of about 28 DU

ACPD
15, 9203–9252, 2015

are observed with IASI. Backtrajectories performed with the HYSPLIT trajectory model (Draxler and Rolph; Rolph) show that the 3 km-altitude air masses located in this area originate from altitudes between 5 and 7 km the day before from North China and Inner Mongolia (Fig. S1 in the Supplement). The tropopause height was around 7–8 km on 5 May 2008 for these regions (Fig. 2h). This means that the air masses reaching Northeast of Tokyo at 3 km on 6 May have a UTLS origin and transport ozone-rich air into the lower troposphere. Thus, we show that the downward transport from the UTLS affects ozone concentrations in the lower troposphere for specific regions on the southeastern flank of the weather system in this case, whereas the perturbation of the tropopause associated to this system influence upper and lower tropospheric ozone over larger areas in the vicinity of the low.

4.2 Influence of high-pressure system on tropospheric ozone distribution over NCP

Lower tropospheric ozone columns as large as 30 DU are observed over NCP on 5 and 6 May 2008 (Fig. 3b and c). The CO columns observed with IASI show also enhanced values over NCP (Fig. 3e and f). The correlation calculated between CO and lower tropospheric ozone columns for a square region including NCP (35–41° N, 114–122° E) is 0.6 on 5 May. If one considers CO as a pollution tracer, this strongly suggests the anthropogenic origin of ozone enhancement observed with IASI in the lower troposphere. In this case, the upper tropospheric ozone column does not show enhanced values over NCP (Fig. 3h and i). The lower troposphere is then not on the direct influence of the UTLS as it was the case for the situation discussed in Sect. 4.1. Figure 5 shows the vertical sections of ozone concentrations for the latitudes of 39, 37, and 35° N on 5 May 2008. At 39° N, the vertical section crosses the NCP in the region of Beijing between 110 and 120° E and also the southern part of the region impacted by the frontal activity (North of Korea peninsula). In this latter case, the free and the upper troposphere presents large ozone concentrations likely due to the downward transport of air masses from the upper troposphere as discussed in the previous section. On

ACPD
15, 9203–9252, 2015

the contrary, the large ozone concentrations over the Beijing region are only observed below 6 km. Ozone concentrations for higher altitude are significantly smaller. The vertical sections of ozone concentration at 35 and 37° N (Fig. 5) show also that ozone enhancements observed over NCP are localized mainly within the lower troposphere, suggesting again the anthropogenic origin of the observed ozone. It is also worth noting that high ozone concentrations were frequently observed from in situ measurements at an altitude of 1.5–2 km above Beijing during April–May (Huang et al., 2014). To investigate if our hypothesis on the anthropogenic origin of the ozone enhancement in this case is valid, we examine the meteorological situation over NCP. On 5 May 2008, an anticyclone is forming over Central East China and the North China Plain inducing cloud free situation and increasing radiation. The northwesterly winds reaching NCP change progressively to southwesterly winds from 4 to 6 May with low winds and then a stagnant situation on 5 May (Fig. 2a–c). This leads to a situation favorable to the accumulation of primary pollutants over NCP and to the photochemical production of ozone due both to local emissions and to the regional transport of pollutants. The ozone and CO enhancements observed from IASI over NCP on 5 and 6 May are then likely due to the photochemical transformation of primary pollutants emitted over NCP.

5 Case study of 11–16 May 2008: combined contributions of anthropogenic and stratospheric sources over NCP and pollution transport

A second episode of high ozone is observed in the lower troposphere with IASI over North China Plain (NCP) from 11 to 16 May 2008. This episode is associated with a cut-off low-pressure system forming on 11 May over Inner Mongolia and moving to the East the days after. From 14 May, the meteorological regime changes over NCP with warmer air masses settling within an anticyclonic situation. In this section, we examine the influence of the meteorological situation on the distribution of lower and upper tropospheric ozone with a particular focus on NCP. Figures 6 and 7 describe the meteorological situation for the entire period. Figures 8 and 9 display the lower and

ACPD
15, 9203–9252, 2015

upper tropospheric ozone columns observed with IASI as well as the total CO columns, also observed with IASI, and the PV averaged between 300 and 500 hPa, taken at the coordinates of IASI pixels. Note that the reader is referred to Fig. 1 for geographical information on East Asia used in the following.

5.1 11–13 May: NCP under the direct influence of the cut-off low

On 11 May 2008, a cut-off low is forming over Inner Mongolia north to the polar jet, which is situated as low as 35° N latitude (Fig. 6a and d). The cut-off low is not yet completely dissociated from the polar reservoir. A band of upper tropospheric columns larger than 40 DU is observed by IASI between 35 and 45° N (Fig. 8g) and associated to a band of PV values larger than 1.6 PVU (Fig. 8j) and a band of tropopauses lower than 9 km (Fig. 6g). The lower tropospheric ozone columns do not show a clear enhancement for the same latitude band. The largest values are observed over the Sea of Japan and the north of Japan. On that day, the perturbation of the tropopause affects the upper tropospheric ozone but only moderately the lower tropospheric ozone.

On 12 May 2008, the cut-off low is well dissociated from the western current (Fig. 6e) and its center reaches the Bohai Sea (Fig. 6b). Upper tropospheric ozone columns larger than 45 DU are retrieved all around the cut-off low. They are correlated with low tropopauses (Fig. 6h) and PV values larger than 1.6 PVU especially on the western flank of the low (Fig. 8k). This indicates a reversible subsiding transfer of ozone in the UTLS. IASI observes lower tropospheric ozone columns larger than 32 DU, especially in the southwestern part of the low, just above NCP (Fig. 8b). The subsiding transfer of ozone due to the tropopause perturbation seems to affect significantly the lower tropospheric ozone. In order to investigate the area where irreversible transfer may occur, we analyze the PV at different pressure levels. Figure 10a shows that layers down to 500 hPa are affected by air masses from the upper troposphere (PV larger than 1.2 PVU) in the southwestern flank of the low over the south of NCP. This suggests that irreversible ozone transfer due to the downward transport of air from the UTLS to the lower troposphere likely contributes to the ozone enhancement observed in the

ACPD
15, 9203–9252, 2015

lower troposphere in this region in addition to the tropopause perturbation. However, Fig. 8e shows that IASI CO columns are also enhanced in the NCP region and partly correlated with the enhanced ozone columns. This indicates that pollution likely plays a concomitant role in the ozone enhancement in that case.

On 13 May 2008, the centre of the cut-off low moves slightly to the East and reaches the Yellow Sea (Fig. 6c). As for the previous day, large upper and lower tropospheric ozone columns are observed with IASI in the vicinity of the low (Fig. 8c and i) in good correlation with the low tropopauses (Fig. 6i) and the large PV values (Fig. 8l). The regions of enhanced ozone are then under the influence of the tropopause perturbation induced by the low with a stronger influence on the southern flank of the low. The analysis of the PV at different pressure levels shows moderate PV values (between 0.8 and 1 PVU) around 31° N between 117 and 122° E (Fig. 10b) where large ozone is observed in the lower troposphere (Fig. 8c). The downward transport of ozone-rich air seems less effective than the previous day. On the same time, a strong enhancement of CO columns is observed over NCP (Fig. 8f) in good spatial correlation with ozone enhancement observed in the lower troposphere. Once again, the pollution seems to play a concomitant role to explain the ozone distribution in the lower troposphere.

5.2 14 May: transition between a cyclonic and an anticyclonic situation

On 14 May 2008, the cut-off low shifts to the Sea of Japan (Fig. 7a). As for the previous days of the period, the regions (Japan, Korea and North China) showing the largest upper tropospheric columns (Fig. 9g) coincide with the regions presenting low tropopause heights (Fig. 7g). The largest PV values affect an area less extended and situated on the southeastern flank of the low, mainly over the Sea of Japan (Fig. 9j). The lower tropospheric columns show a strong enhancement of ozone for the same region of the Sea of Japan (Fig. 9a). This region is then clearly under the influence of the UTLS.

Over China, an anticyclonic situation starts to develop south to NCP inducing a change in the wind regime and warmer conditions from 14 May (Fig. 7a). Large CO columns and lower tropospheric ozone columns are retrieved with IASI over NCP

ACPD
15, 9203–9252, 2015

(Fig. 9a). Unlike the previous days, the absence of concomitant large PV values and low tropopause heights indicates that the large lower tropospheric ozone concentrations are disconnected from the UTLS polar ozone reservoir. The large ozone values are likely attributed to photochemical production of ozone over the highly polluted region of NCP. Figure 11 shows the vertical section of ozone concentrations retrieved with IASI at different latitudes. Very large ozone concentrations are retrieved for the entire free and upper troposphere in the eastern part of the sections (Fig. 11). This corresponds to the region over the Sea of Japan under the direct influence of the cut-off low and then greatly influenced by the UTLS. The situation is different over NCP: ozone concentrations in the upper troposphere are moderate and a distinct maximum in the lower troposphere is well visible, especially in the south of NCP at 35° N (Fig. 11). This associated with CO enhancement suggest that the ozone enhancement observed with IASI over NCP is of anthropogenic origin.

5.3 15–16 May: NCP under anticyclonic influence

On 15 May 2008, strong enhancements of CO and lower tropospheric ozone are observed with IASI over the entire NCP (Fig. 9b and e). Both CO and O_3 increase compared to the previous day. The anticyclone is well settled over China leading to a stagnant situation with low winds all over NCP (Fig. 7b). This situation is favorable to the accumulation of pollutants and then to the photochemical production of ozone. Figure 12 shows the vertical section of ozone concentrations retrieved with IASI at different latitudes. The ozone enhancement is located within the lower troposphere. This strongly suggests that the ozone enhancement is related to photochemical production of ozone from emitted pollutants in NCP. On 16 May 2008, the situation is cloudier over NCP (Fig. 9c). But still large lower tropospheric ozone columns and CO columns are observed in good correlation (Fig. 9c and f), suggesting once again the same origin for ozone and CO.

Enhanced ozone in the lower troposphere is also retrieved on 15 and 16 May in North China following the Shenyang–Harbin axis (Fig. 9b and c). On 15 May, this ozone en-

ACPD
15, 9203–9252, 2015

hancement in the lower troposphere is associated with both large upper tropospheric ozone columns and large CO columns (at least in the southern part of this axis), suggesting a contribution from both the UTLS and the photochemical production to the lower tropospheric column. On 16 May, large CO columns extent more to Harbin and the contribution from the UTLS is limited as the upper tropospheric ozone columns are smaller. The presence of large CO columns indicates that the enhancement of lower tropospheric ozone observed in this region is likely due to pollution.

5.4 Evidence of transboundary transport within the cut-off low

On 13 and 14 May, large CO and O_3 columns are retrieved from IASI over Yellow Sea and over the Sea of Japan in the southern flank of the cut-off low-pressure system (Figs. 8c and 9a). Fairly strong westerly winds are present at 850 hPa in the same region suggesting a possible advection of air masses from NCP towards Japan associated with the weather system (Figs. 6c and 7a). In order to evaluate if the weather system may have contributed to transport the pollutants (O_3 and CO), we perform backtrajectories on 13 May for an area south to Korea (Fig. S2). The 3 km air masses originate from the boundary layer over NCP on 11 May. They have been uplifted and transported at an altitude between 3 and 4 km the days after (Fig. S2). In order to investigate if the pollutant uplifting on 11 May occurs on a region more extended than those shown on Fig. S2, we examined two meteorological variables that indicate possible ascending motion of air masses: the convective available potential energy (CAPE) and the vertical velocity. Figure 13 shows that the CAPE is significant on the inside eastern flank of the cut-off low and that negative vertical velocities, i.e ascending winds, are present from the surface up to 300 hPa (Fig. 13 shows only the vertical velocity at 700 hPa as an example). In addition, backtrajectories performed on 11 May indicate that most of the air masses between 38–40° N and 116–117° E at 3 km originate from the atmospheric layers below 1 km and circulate over NCP during the previous 24 h (Fig. S3). This evidences that pollutants (CO and O_3) have been uplifted from the boundary layer into the free troposphere over NCP and then exported towards Japan by the cut-off low.

ACPD
15, 9203–9252, 2015

We can assume that part of the large lower tropospheric ozone observed is then due to the transport of ozone produced over NCP but also to ozone produced during the transport.

6 Discussion

The analysis of two case studies involving low-pressure systems in May 2008 shows the importance of the associated tropopause perturbations and the potential associated ozone transfer (downward transport from the upper troposphere within the dry airstream behind the cold front or in the vicinity of cut-off low-pressure systems) in order to explain the large quantities of ozone observed with IASI in the upper troposphere but also in the lower troposphere. The vertical resolution of IASI does not allow a clear discrimination between the different processes involved in such weather systems. However, the two case studies illustrate also the key role of photochemically produced ozone over large polluted regions such as NCP. The ozone enhancement occurs usually in strong coincidence with CO enhancement when anticyclonic conditions settle. Using CO as a pollutant tracer, we can conclude that most of the ozone enhancement observed in this case is due to photo-oxidation of pollutants emitted over NCP. The satellite observations are limited to cloud-free observations or to observations only weakly contaminated by clouds ($< 15\,\%$). The anticyclonic situations are then preferentially sampled due to the low cloud cover in such situations. This does not mean that ozone enhancement associated to pollution occurs only when high-pressure systems are settled. Indeed, we show that the anthropogenic source can contribute concomitantly with the stratospheric source to explain the ozone enhancement observed in the vicinity of the cut-off low case study detailed in Sect. 5, implying that large ozone concentrations are present not only in stable meteorological (anticyclonic) situations. In addition, we also show with satellite observations, the role of such meteorological systems in the transboundary transport of pollution on a daily basis.

ACPD
15, 9203–9252, 2015

The succession of low- and high-pressure systems plays a key role in explaining the day-to-day variability of lower tropospheric ozone over North East Asia. In May 2008, 5 events covering 2–3 days each and leading to significant ozone enhancement in the lower troposphere have been identified. In order to evaluate the regions of influence of the frontal and cyclonic activity on the ozone distribution, we calculated monthly mean of lower and upper tropospheric ozone columns (Fig. 14) as well as the monthly mean of PV between 300 and 500 hPa (Fig. 15). The monthly mean are given with a 0.25° × 0.25° horizontal resolution. The upper tropospheric ozone columns, the most affected by the tropopause perturbations and the ozone transfer from the lower stratosphere associated with frontal activity, and the PV distribution provide a view of the region of influence of the frontal and cyclonic activity in terms of ozone enhancement. This region is located north to 40° N and extends from Inner Mongolia to North China and North of Japan. The upper tropospheric ozone column (6 to 12 km) used in this study is well correlated with the PV distribution and can be used as a proxy to identify the regions influenced by tropopause perturbations and ozone transfer. Below 40° N, the influence of the frontal and cyclonic activity on lower tropospheric ozone decreases.

In order to investigate the role of pollution in enhanced lower tropospheric ozone columns observed with IASI, we compare monthly distribution of lower tropospheric ozone columns with the distribution of total CO columns and tropospheric NO_2 columns, often used as anthropogenic sources tracers (Fig. 14). The NO_2 tropospheric columns are those observed by the GOME-2 instrument operating on the same satellite platform than the IASI instrument (Boersma et al., 2004) (http://www.temis.nl/airpollution/no2.html). All the regions of continental East Asia (NCP, Sichuan Basin, North China...) showing large NO_2 tropospheric columns and then indicating large anthropogenic sources present large total CO columns and also large lower tropospheric ozone columns (Fig. 14). A correlation of 0.62 over the entire domain between IASI lower tropospheric ozone and IASI total CO suggests that anthropogenic sources significantly contribute to the ozone observed in the lower troposphere with IASI. North China Plain, Yangtze River Delta (near Shanghai) and the Hubei province (Wuhan

ACPD
15, 9203–9252, 2015

region) are the regions the most impacted by pollution according to the satellite observations. Large lower tropospheric ozone columns are observed over North China corresponding to the industrialised Shenyang–Harbin axis also visible in CO and NO_2 observations (Fig. 14). However, the ozone plume extends more to the west compared to the CO and NO_2 plumes. This may be explained by the influence of the UTLS, which is larger all over the northern part of the domain. Lower tropospheric columns of ozone might also be overestimated during the retrieval because the region is partly arid. Indeed, the ozone retrieval can be partly impacted in regions of low emissivity, as it is likely the case in the northwestern part of the domain. In the southern part of the domain, enhanced lower tropospheric ozone columns are observed in the Sichuan Basin and the Guangdong province in coincidence with enhanced CO and NO_2 columns. In this latter region, closer to the equator, the distance between two successive swaths of IASI increases. Then, the spatial coverage of IASI decreases and it is then less easy to follow the daily variability of ozone. Moreover, the maximum of sensitivity of IASI ozone retrievals in the tropics is usually higher in altitude, around 5 km (Dufour et al., 2012). IASI observations are then less suitable to efficiently monitor pollution in such cases.

7 Conclusion

The possibility with IASI to identify contribution from the lower and the upper tropospheric ozone with a large spatial coverage offers new insight on the synoptic processes controlling tropospheric ozone. Indeed, we show that the state-of-the-art IASI ozone product used in this study has good performances in terms of accuracy and precision, especially in the lower troposphere. Validation against ozonesonde measurements shows small biases (−0.6 DU or −2.8 %) and reasonable error estimates (2.8 DU or 14 %) for the lower tropospheric ozone columns.

We show evidence that the succession of low- and high-pressure systems strongly influences the day-to-day variability of lower tropospheric ozone over North East Asia during springtime. We show that the tropopause perturbations associated with the

ACPD
15, 9203–9252, 2015

ozone transfer from the lower stratosphere to the troposphere occurring in the vicinity of low-pressure systems (e.g. behind cold fronts) affect the free and lower tropospheric ozone over large regions with different examples taken in May 2008. We determine the region of influence of such system, located mainly above 40° N but with some particular intense events (cut-off low from 11 to 13 May 2008) impacting southern regions such as NCP for few days. We show also that such systems, with potential convective capacity, when they travel over highly polluted regions, play also a role in the transboundary transport of pollutants.

In addition to the stratospheric influence on tropospheric ozone in the northern part of the domain, most of the enhanced lower tropospheric ozone columns are observed in regions mainly impacted by strong pollution level. Significant correlations between CO (used as a pollution tracer) and ozone in the lower troposphere have been found. Moreover, the analysis of vertical sections of ozone concentrations over NCP indicates that ozone concentrations are enhanced only in the lower troposphere in such regions. This suggests the anthropogenic origin of the observed ozone enhancements. Finally, we show that being able to retrieve semi-independent columns of ozone from the surface up to 12 km and having simultaneously CO columns from IASI provide a powerful dataset to depict the processes controlling tropospheric ozone enhancement at synoptic scales.

In the largest plumes, the stratospheric source is often concomitant with the pollution source and then both influence lower tropospheric ozone and contribute to ozone enhancements. Due to the limited vertical resolution of IASI and its limited sensitivity to surface ozone, it is not possible to identify on a fine vertical grid the region of influence in altitude of these different sources. Advanced satellite products coupling UV and IR information such as the recent IASI+GOME-2 product (Cuesta et al., 2013) as well as the next generation of satellite instruments (Crevoisier et al., 2014; Veefkind et al., 2012) should help improving the vertical observation of lower tropospheric ozone. These observations combined with modelling studies would help identifying these regions.

ACPD
15, 9203–9252, 2015

The Supplement related to this article is available online at doi:10.5194/acpd-15-9203-2015-supplement.

Acknowledgements. We acknowledge the Institut für Meteorologie und Klimaforschung (IMK), Karlsruhe, Germany, for a licence to use the KOPRA radiative transfer model. This study was supported by the French Space Agency – CNES (project "IASI-TOSCA"). The IASI mission is a joint mission of Eumetsat and the Centre National d'Etudes Spatiales (CNES, France). The IASI L1 data are distributed in near real time by Eumetsat through the Eumetcast system distribution.We acknowledge the Ether CNES/CNRS-INSU database (http://www.pole-ether.fr) for providing access to IASI Level 1 data. We acknowledge the LATMOS/ULB for the provision of IASI CO total columns through the Ehter CNES/CNRS-INSU database. The authors gratefully acknowledge the NOAA Air Resources Laboratory (ARL) for the provision of the HYSPLIT transport and dispersion model and/or READY website (http://www.ready.noaa.gov) used in this publication. We acknowledge the free use of tropospheric NO_2 column data from the GOME-2 sensor from www.temis.nl. The ozonesonde data used in this study were mainly provided by the World Ozone and Ultraviolet Data Centre (WOUDC), the Southern Hemisphere Additional Ozonesondes (SHADOZ), and the Global Monitoring Division (GMD) of NOAA's Earth System Research Laboratory and are publicly available (see http://www.woudc.org, http://croc.gsfc.nasa.gov/shadoz, http://www.esrl.noaa.gov/gmd). The authors thank all those responsible for the WOUDC, SHADOZ, and GMD measurements and archives for making the ozonesonde data available.

References

Ancellet, G., Beekmann, M., and Papayannis, A.: Impact of a cut-off low development on downward transport of ozone in the troposphere, J. Geophys. Res., 99, 3451–3468, 1994.

Barret, B., Le Flochmoen, E., Sauvage, B., Pavelin, E., Matricardi, M., and Cammas, J. P.: The detection of post-monsoon tropospheric ozone variability over south Asia using IASI data, Atmos. Chem. Phys., 11, 9533–9548, doi:10.5194/acp-11-9533-2011, 2011.

Bethan, S., Vaughan, G., and Reid, S. J.: A comparison of ozone and thermal tropopause heights and the impact of tropopause definition on quantifying the ozone content of the troposphere, Q. J. Roy. Meteor. Soc., 122, 929–944, doi:10.1002/qj.49712253207, 1996.

ACPD
15, 9203–9252, 2015

Bethan, S., Vaughan, G., Gerbig, C., Volz-Thomas, A., Richer, H., and Tiddeman, D. A.: Chemical air mass differences near fronts, J. Geophys. Res., 103, 13413–13434, 1998.
Bey, I., Jacob, D. J., Logan, J. A., and Yantosca, R. M.: Asian chemical outflow to the Pacific in spring: origins, pathways, and budgets, J. Geophys. Res., 106, 23097–23113, 2001.
Boersma, K. F., Eskes, H. J., and Brinksma, E. J.: Error analysis for tropospheric NO_2 retrieval from space, J. Geophys. Res., 109, D04311, doi:10.1029/2003JD003962, 2004.
Bolton, D.: The computation of equivalent potential temperature, Mon. Weather Rev., 108, 1046–1053, 1980.
Boynard, A., Clerbaux, C., Coheur, P.-F., Hurtmans, D., Turquety, S., George, M., Hadji-Lazaro, J., Keim, C., and Meyer-Arnek, J.: Measurements of total and tropospheric ozone from IASI: comparison with correlative satellite, ground-based and ozonesonde observations, Atmos. Chem. Phys., 9, 6255–6271, doi:10.5194/acp-9-6255-2009, 2009.
Carmichael, G. R., Uno, I., Phadnis, M. J., Zhang, Y., and Sunwoo, Y.: Tropospheric ozone production and transport in the springtime in east Asia, J. Geophys. Res., 103, 10649–10671, 1998.
Chan, C. K. and Yao, X.: Air pollution in mega cities in China, Atmos. Environ., 42, 1–42, 2008.
Clarisse, L., R'Honi, Y., Coheur, P.-F., Hurtmans, D., and Clerbaux, C.: Thermal infrared nadir observations of 24 atmospheric gases, Geophys. Res. Lett., 38, L10802, doi:10.1029/2011GL047271, 2011.
Clerbaux, C., Boynard, A., Clarisse, L., George, M., Hadji-Lazaro, J., Herbin, H., Hurtmans, D., Pommier, M., Razavi, A., Turquety, S., Wespes, C., and Coheur, P.-F.: Monitoring of atmospheric composition using the thermal infrared IASI/MetOp sounder, Atmos. Chem. Phys., 9, 6041–6054, doi:10.5194/acp-9-6041-2009, 2009.
Coheur, P.-F., Barret, B., Turquety, S., Hurtmans, D., Hadji-Lazaro, J., and Clerbaux, C.: Retrieval and characterization of ozone vertical profiles from a thermal infrared nadir sounder, J. Geophys. Res., 110, D24303, doi:10.1029/2005JD005845, 2005.
Cooper, O. R., Moody, J. L., Davenport, J. C., Oltmans, S. J., Johnson, B. J., Chen, X., Shepson, P. B., and Merrill, J. T.: Influence of springtime weather systems on vertical ozone distribution over three North American sites, J. Geophys. Res., 103, 22001–22013, 1998.
Cooper, O. R., Moody, J. L., Parrish, D. D., Trainer, M., Holloway, J. S., Hübler, G., Fehsenfeld, F. C., and Stohl, A.: Trace gas composition of midlatitude cyclones over the western North Atlantic Ocean: a seasonal comparison of O_3 and CO, J. Geophys. Res., 107, ACH 2-1–ACH 2-12, doi:10.1029/2001JD000902, 2002a.

ACPD
15, 9203–9252, 2015

Cooper, O. R., Moody, J. L., Parrish, D. D., Trainer, M., Ryerson, T. B., Holloway, J. S., Hübler, G., Fehsenfeld, F. C., and Evans, M. J.: Trace gas composition of midlatitude cyclones over the western North Atlantic Ocean: a conceptual model, J. Geophys. Res., 107, ACH 1-1–ACH 1-13, doi:10.1029/2001JD000901, 2002b.

Cooper, O. R., Forster, C., Parrish, D., Trainer, M., Dunlea, E., Ryerson, T., Hübbler, G., Fehsenfeld, F., Nicks, D., Holloway, J., de Gouw, J., Warneke, C., Roberts, J. M., Flocke, F., and Moody, J.: A case study of transpacific warm conveyor belt transport: influence of merging airstreams on trace gas import to North America, J. Geophys. Res., 109, D23S08, doi:10.1029/2003JD003624, 2004.

Crevoisier, C., Clerbaux, C., Guidard, V., Phulpin, T., Armante, R., Barret, B., Camy-Peyret, C., Chaboureau, J.-P., Coheur, P.-F., Crépeau, L., Dufour, G., Labonnote, L., Lavanant, L., Hadji-Lazaro, J., Herbin, H., Jacquinet-Husson, N., Payan, S., Péquignot, E., Pierangelo, C., Sellitto, P., and Stubenrauch, C.: Towards IASI-New Generation (IASI-NG): impact of improved spectral resolution and radiometric noise on the retrieval of thermodynamic, chemistry and climate variables, Atmos. Meas. Tech., 7, 4367–4385, doi:10.5194/amt-7-4367-2014, 2014.

Cuesta, J., Eremenko, M., Liu, X., Dufour, G., Cai, Z., Höpfner, M., von Clarmann, T., Sellitto, P., Foret, G., Gaubert, B., Beekmann, M., Orphal, J., Chance, K., Spurr, R., and Flaud, J.-M.: Satellite observation of lowermost tropospheric ozone by multispectral synergism of IASI thermal infrared and GOME-2 ultraviolet measurements over Europe, Atmos. Chem. Phys., 13, 9675–9693, doi:10.5194/acp-13-9675-2013, 2013.

de Laat, A. T. J., Aben, I., and Roelofs, G. J.: A model perspective on total tropospheric O_3 column variability and implications for satellite observations, J. Geophys. Res., 110, D13303, doi:10.1029/2004JD005264, 2005.

Dee, D. P., Uppala, S. M., Simmons, A. J., Berrisford, P., Poli, P., Kobayashi, S., Andrae, U., Balmaseda, M. A., Balsamo, G., Bauer, P., Bechtold, P., Beljaars, A. C. M., van de Berg, L., Bidlot, J., Bormann, N., Delsol, C., Dragani, R., Fuentes, M., Geer, A. J., Haimberger, L., Healy, S. B., Hersbach, H., Hólm, E. V., Isaksen, L., Kållberg, P., Köhler, M., Matricardi, M., McNally, A. P., Monge-Sanz, B. M., Morcrette, J.-J., Park, B.-K., Peubey, C., de Rosnay, P., Tavolato, C., Thépaut, J.-N., and Vitart, F.: The ERA-Interim reanalysis: configuration and performance of the data assimilation system, Q. J. Roy. Meteor. Soc., 137, 553–597, doi:10.1002/qj.828, 2011.

Dempsey, F.: Observations of stratospheric O_3 intrusions in air quality monitoring data in Ontario, Canada, Atmos. Environ., 98, 111–122, doi:10.1016/j.atmosenv.2014.08.024, 2014.

ACPD
15, 9203–9252, 2015

Ding, A. J., Wang, T., Thouret, V., Cammas, J.-P., and Nédélec, P.: Tropospheric ozone climatology over Beijing: analysis of aircraft data from the MOZAIC program, Atmos. Chem. Phys., 8, 1–13, doi:10.5194/acp-8-1-2008, 2008.

Ding, A., Wang, T., Xue, L., Gao, J., Stohl, A., Lei, H., Jin, D., Ren, Y., Wang, X., Wei, X., Qi, Y., Liu, J., and Zhang, X.: Transport of north China air pollution by midlatitude cyclones: case study of aircraft measurements in summer 2007, J. Geophys. Res., 114, D08304, doi:10.1029/2008JD011023, 2009.

Doche, C., Dufour, G., Foret, G., Eremenko, M., Cuesta, J., Beekmann, M., and Kalabokas, P.: Summertime tropospheric-ozone variability over the Mediterranean basin observed with IASI, Atmos. Chem. Phys., 14, 10589–10600, doi:10.5194/acp-14-10589-2014, 2014.

Draxler, R. R. and Rolph, G. D.: HYSPLIT (HYbrid Single-Particle Lagrangian Integrated Trajectory) Model access via NOAA ARL READY Website, available at: http://www.arl.noaa.gov/HYSPLIT.php (last access: 23 January 2015), NOAA Air Resources Laboratory, College Park, MD, 2003.

Dufour, G., Eremenko, M., Orphal, J., and Flaud, J.-M.: IASI observations of seasonal and day-to-day variations of tropospheric ozone over three highly populated areas of China: Beijing, Shanghai, and Hong Kong, Atmos. Chem. Phys., 10, 3787–3801, doi:10.5194/acp-10-3787-2010, 2010.

Dufour, G., Eremenko, M., Griesfeller, A., Barret, B., LeFlochmoën, E., Clerbaux, C., Hadji-Lazaro, J., Coheur, P.-F., and Hurtmans, D.: Validation of three different scientific ozone products retrieved from IASI spectra using ozonesondes, Atmos. Meas. Tech., 5, 611–630, doi:10.5194/amt-5-611-2012, 2012.

Edwards, D. P., Emmons, L. K., Hauglustaine, D. A., Chu, A., Gille, J. C., Kaufman, Y. J., P'etron, G., Yurganov, L. N., Giglio, L., Deeter, M. N., Yudin, V., Ziskin, D. C.,Warner, J., Lamarque, J.-F., Francis, G. L., Ho, S. P., Mao, D., Chan, J., and Drummond, J. R.: Observations of carbon monoxide and aerosol from the Terra satellite: Northern Hemisphere variability, J. Geophys. Res. Atmos., 109, D24202, doi:10.1029/2004JD004727, 2004.

Eremenko, M., Dufour, G., Foret, G., Keim, C., Orphal, J., Beekmann, M., Bergametti, G., and Flaud, J.-M.: Tropospheric ozone distributions over Europe during the heat wave in July 2007 observed from infrared nadir spectra recorded by IASI, Geophys. Res. Lett., 35, L18805, doi:10.1029/2008GL034803, 2008.

Fishman, J., Wozniak, A. E., and Creilson, J. K.: Global distribution of tropospheric ozone from satellite measurements using the empirically corrected tropospheric ozone residual tech-

ACPD
15, 9203–9252, 2015

nique: identification of the regional aspects of air pollution, Atmos. Chem. Phys., 3, 893–907, doi:10.5194/acp-3-893-2003, 2003.
Foret, G., Eremenko, M., Cuesta, J., Sellitto, P., Barré, J., Gaubert, B., Coman, A., Dufour, G., Liu, X., Joly, M., Doche, C., and Beekmann, M.: Ozone pollution: what can we see from space? A case study, J. Geophys. Res.-Atmos., 119, 8476–8499, doi:10.1002/2013JD021340, 2014.
George, M., Clerbaux, C., Hurtmans, D., Turquety, S., Coheur, P.-F., Pommier, M., Hadji-Lazaro, J., Edwards, D. P., Worden, H., Luo, M., Rinsland, C., and McMillan, W.: Carbon monoxide distributions from the IASI/METOP mission: evaluation with other space-borne remote sensors, Atmos. Chem. Phys., 9, 8317–8330, doi:10.5194/acp-9-8317-2009, 2009.
Hannan, J. R., Fuelberg, H. E., Crawford, J. H., Sachse, G. W., and Blake, D. R.:Role of wave cyclones in transporting boundary layer air to the free troposphere during the spring 2001 NASA/TRACE-P experiment, J. Geophys. Res., 108, 8782, doi:10.1029/2002JD003105, 2003.
Hayashida, S., Liu, X., Ono, A., Yang, K., and Chance, K.: Observation of ozone enhancement in the lower troposphere over East Asia from a space-borne ultraviolet spectrometer, Atmos. Chem. Phys. Discuss., 15, 2013–2054, doi:10.5194/acpd-15-2013-2015, 2015.
Holton, J. R., Haynes, P. H., McIntyre, M. E., Douglass, A. R., Rood, R. B., and Pfister, L.: Stratosphere–troposphere exchange, Rev. Geophys., 33, 403–439, 1995.
Holton, J. R.: An Introduction to Dynamic Meteorology, 4th edn., Elsevier, New York, 2004.
Huang, J., Liu, H., Crawford, J. H., Chan, C., Considine, D. B., Zhang, Y., Zheng, X., Zhao, C., Thouret, V., Oltmans, S. J., Liu, S. C., Jones, D. B. A., Steenrod, S. D., and Damon, M. R.: Origin of springtime ozone enhancements in the lower troposphere over Beijing: in situ measurements and model analysis, Atmos. Chem. Phys. Discuss., 14, 32583–32627, doi:10.5194/acpd-14-32583-2014, 2014.
Hurtmans, D., Coheur, P.-F., Wespes, C., Clarisse, L., Scharf, O., Clerbaux, C., Hadji-Lazaro, J., George, M., and Turquety, S.: FORLI radiative transfer and retrieval code for IASI, JQSRT, 113, 1391–1408, doi:10.1016/j.jqsrt.2012.02.036, 2012.
Jaffe, D., Anderson, T., Covert, D., Kotchenruther, R., Trost, B., Danielson, J., Simpson, W., Berntsen, T., Karlsdottir, S., Blake, D., Harris, J., Carmichael, G., and Uno, I.: Transport of Asian air pollution to North America, Geophys. Res. Lett., 26, 711–714, 1999.
Lelieveld, J. and Dentener, F. J.: What controls tropospheric ozone?, J. Geophys. Res., 105, 3531–3551, 2000.

ACPD
15, 9203–9252, 2015

Kulawik, S. S., Osterman, G., Jones, D. B. A., and Bowman, K. W.: Calculation of altitude-dependent Tikhonov constraints for TES nadir retrievals, IEEE T. Geosci. Remote, 44, 1334–1342, 2006.

Li, J., Wang, Z., Akimoto, H., Gao, C., Pochanart, P., and Wang, X.: Modeling study of ozone seasonal cycle in lower troposphere over east Asia, J. Geophys. Res., 112, D22S25, doi:10.1029/2006JD008209, 2007.

Liang, Q., Jaeglé, L., Jaffe, D. A., Weiss-Penzias, P., Heckman, A., and Snow, J. A.: Long-range transport of Asian pollution to the northeast Pacific: seasonal variations and transport pathways of carbon monoxide, J. Geophys. Res., 109, D23S07, doi:10.1029/2003JD004402, 2004.

Lin, J., Pan, D., and Zhang, R.-X.: Trend and interannual variability of Chinese air pollution since 2000 in association with socioeconomic development: a brief overview, Atmospheric and Oceanic Science Letters, 6, 84–89, 2013.

Lin, M., Holloway, T., Carmichael, G. R., and Fiore, A. M.: Quantifying pollution inflow and outflow over East Asia in spring with regional and global models, Atmos. Chem. Phys., 10, 4221–4239, doi:10.5194/acp-10-4221-2010, 2010.

Liu, H., Jacob, D. J., Bey, I., Yantosca, R. M., Duncan, B. N., and Sachse, G. W.: Transport pathways for Asian pollution outflow over the Pacific: interannual and seasonal variations, J. Geophys. Res., 108, 8786, doi:10.1029/2002JD003102, 2003.

Liu, X., Chance, K., and Kurosu, T. P.: Improved ozone profile retrievals from GOME data with degradation correction in reflectance, Atmos. Chem. Phys., 7, 1575–1583, doi:10.5194/acp-7-1575-2007, 2007.

Liu, X., Bhartia, P. K., Chance, K., Spurr, R. J. D., and Kurosu, T. P.: Ozone profile retrievals from the Ozone Monitoring Instrument, Atmos. Chem. Phys., 10, 2521–2537, doi:10.5194/acp-10-2521-2010, 2010.

Liu, C. X., Liu, Y., Liu, X., and Chance, K.: Dynamical and chemical features of a cutoff low over Northeast China in July 2007: results from satellite measurements and reanalysis, Adv. Atmos. Sci., 30, 525–540, doi:10.1007/s00376-012-2086-8, 2013.

Mari, C., Evans, M. J., Palmer, P. I., Jacob, D. J., and Sachse, G. W.: Export of Asian pollution during two cold front episodes of the TRACE-P experiment, J. Geophys. Res., 109, D15S17, doi:10.1029/2003JD004307, 2004.

Mauzerall, D. L., Narita, D., Akimoto, H., Horowitz, L., Walters, S., Hauglustaine, D. A., and Brasseur, G.: Seasonal characteristics of tropospheric ozone production and mixing ratios

ACPD
15, 9203–9252, 2015

over East Asia: a global three-dimensional chemical transport model analysis, J. Geophys. Res., 105, 17895–17910, doi:10.1029/2000JD900087, 2000.
McMillan, W. W., Pierce, R., Sparling, L. C., Osterman, G., McCann, K., Fischer, M. L., Rappenglueck, B., Newton, R., Turner, D. D., Kittaka, C., Evans, K., Biraud, S., Lefer, B., Andrews, A., and Oltmans, S.: An observational and modeling strategy to investigate the impact of remote sources on local air quality: a Houston, Texas case study from TEXAQS II, J. Geophys. Res.-Atmos., 115, D01301, doi:10.1029/2009JD011973, 2010.
McPeters, R. D., Labow, G. J., and Logan, J. A.: Ozone climatological profiles for satellite retrieval algorithms, J. Geophys. Res., 112, D05308, doi:10.1029/2005JD006823, 2007.
Monks, P. S.: A review of the observations and origins of the spring ozone maximum, Atmos. Environ., 34, 3545–3561, 2000.
Monks, P. S.: Gas-phase radical chemistry in the troposphere, Chem. Soc. Rev., 34, 376–395, 2005.
Monks, P. S., Archibald, A. T., Colette, A., Cooper, O., Coyle, M., Derwent, R., Fowler, D., Granier, C., Law, K. S., Stevenson, D. S., Tarasova, O., Thouret, V., von Schneidemesser, E., Sommariva, R., Wild, O., and Williams, M. L.: Tropospheric ozone and its precursors from the urban to the global scale from air quality to short-lived climate forcer, Atmos. Chem. Phys. Discuss., 14, 32709–32933, doi:10.5194/acpd-14-32709-2014, 2014.
Nakatani, A., Kondo, S., Hayashida, S., Nagashima, T., Sudo, K., Liu, X., Chance, K., and Hirota, I.: Enhanced mid-latitude tropospheric column ozone over East Asia: couple effects of stratospheric ozone intrusion and anthropogenic sources, J. Meteorol. Soc. Jpn., 90, 207–222, 2012.
Oshima, N., Koike, M., Nakamura, H., Kondo, Y., Takegawa, N., Miyazaki, Y., Blake, D. R., Shirai, T., Kita, K., Kawakami, S., and Ogawa, T.: Asian chemical outflow to the Pacific in late spring observed during the PEACE-B aircraft mission, J. Geophys. Res., 109, D23S05, doi:10.1029/2004JD004976, 2004.
Richter, A., Burrows, J. P., Nub, H., Granier, C., and Niemeier, U.: Increase in tropospheric nitrogen dioxide over China observed from space, Nature, 437, 129–132, 2005.
Rodgers, C. D.: Inverse Methods for Atmospheric Sounding: Theory and Practice, vol. 2, World Scientific Publications, Series on Atmospheric, Ocean, Planet. Phys., Singapore, 2000.
Rolph, G. D.: Real-time Environmental Applications and Display sYstem (READY) Website, available at: http://www.ready.noaa.gov (23 January 2015), NOAA Air Resources Laboratory, College Park, MD, 2003.

ACPD
15, 9203–9252, 2015

Safieddine, S., Clerbaux, C., George, M., Hadji-Lazaro, J., Hurtmans, D., Coheur, P.-F., Wespes, C., Loyola, D., Valks, P., and Hao, N.: Tropospheric ozone and nitrogen dioxide measurements in urban and rural regions as seen by IASI and GOME-2, J. Geophys. Res.-Atmos., 118, 10555–10566, doi:10.1002/jgrd.50669, 2013.

Schuepbach, E., Davies, T. D., and Massacand, A. C.: An usual springtime ozone episode at high elevation in the Swiss Alps: contributions both from cross-tropopause exchange and from the boundary layer, Atmos. Environ., 33, 1735–1744, 1999.

Seinfeld, J. H. and Pandis, S. N.: Atmospheric Chemistry and Physics, from Air Pollution to Climate Change, John Wiley & Sons Inc., Toronto, Canada, 1997.

Stevenson, D. S., Dentener, F. J., Schultz, M. G., Ellingsen, K., van Noije, T. P. C., Wild, O., Zeng, G., Amann, M., Atherton, C. S., Bell, N., Bergmann, D. J., Bey, I., Butler, T., Cofala, J., Collins, W. J., Derwent, R. G., Doherty, R. M., Drevet, J., Eskes, H. J., Fiore, A. M., Gauss, M., Hauglustaine, D. A., Horowitz, L. W., Isaksen, I. S. A., Krol, M. C., Lamarque, J. F., Lawrence, M. G., Montanaro, V., Muller, J. F., Pitari, G., Prather, M. J., Pyle, J. A., Rast, S., Rodriguez, J. M., Sanderson, M. G., Savage, N. H., Shindell, D. T., Strahan, S. E., Sudo, K., and Szopa, S.: Multimodel ensemble simulations of present-day and near-future tropospheric ozone, J. Geophys. Res.-Atmos., 111, D08301, doi:10.1029/2005jd006338, 2006.

Stiller, G. P. (Ed.): The Karlsruhe Optimized and Precise Radiative Transfer Algorithm (KOPRA), vol. FZKA 6487 of Wissenschaftliche Berichte, with contributions from v. Clarmann, T., Dudhia, A., Echle, G., Funke, B., Glatthor, N., Hase, F., Höpfner, M., Kellmann, S., Kemnitzer, H., Kuntz, M., Linden, A., Linder, M., Stiller, G. P., and Zorn, S., Forschungszentrum Karlsruhe, Karlsruhe, Germany, 2000.

Tikhonov, A.: On the solution of incorrectly stated problems and a method of regularisation, Dokl. Akad. Nauk SSSR, 151, 501–504, 1963.

Veefkind, J. P., Aben, I., McMullan, K., Förster, H., de Vries, J., Otter, G., Claas, J., Eskes, H. J., de Haan, J. F., Kleipool, Q., van Weele, M., Hasekamp, O., Hoogeveen, R., Landgraf, J., Snel, R., Tol, P., Ingmann, P., Voors, R., Kruisinga, B., Vink, R., Visser, H., and Levelt, P. F.: TROPOMI on the ESA Sentinel-5 precursor: a GMES mission for global observations of the atmospheric composition for climate, air quality and ozone layer applications, Remote Sens. Environ., 120, 70–83, doi:10.1016/j.rse.2011.09.027, 2012.

Wang, T., Wei, X. L., Ding, A. J., Poon, C. N., Lam, K. S., Li, Y. S., Chan, L. Y., and Anson, M.: Increasing surface ozone concentrations in the background atmosphere of Southern China, 1994–2007, Atmos. Chem. Phys., 9, 6217–6227, doi:10.5194/acp-9-6217-2009, 2009.

ACPD
15, 9203–9252, 2015

Wang, Y., Konopka, P., Liu, Y., Chen, H., Müller, R., Plöger, F., Riese, M., Cai, Z., and Lü, D.: Tropospheric ozone trend over Beijing from 2002–2010: ozonesonde measurements and modeling analysis, Atmos. Chem. Phys., 12, 8389–8399, doi:10.5194/acp-12-8389-2012, 2012.
WHO: Review of Evidence on Health Aspects of Air Pollution – REVIHAAP Project: Final Technical Report, WHO Regional Office for Europe, Copenhagen, Denmark, 2013.
WMO: International List of Selected and Supplementary Ships, 3, WMO 47 (WMO/OMM 47, TP. 18), Geneva, Switzerland, 143 pp., 1957.
Worden, H. M., Logan, J. A., Worden, J. R., Beer, R., Bowman, K., Clough, S. A., Eldering, A., Fisher, B. M., Gunson, M. R., Herman, R. L., Kulawik, S. S., Lampel, M. C., Luo, M., Megretskaia, I. A., Osterman, G. B., and Shephard, M. W.: Comparisons of Tropospheric Emission Spectrometer (TES) ozone profiles to ozonesondes: methods and initial results, J. Geophys. Res., 112, D03309, doi:10.1029/2006JD007258, 2007.
Yamaji, K., Ohara, T., Uno, I., Tanimoto, H., Kurokawa, J., and Akimoto, H.: Analysis of the seasonal variation of ozone in the boundary layer in East Asia using the Community Multiscale Air Quality model: what controls surface ozone levels over Japan?, Atmos. Environ., 40, 1856–1868, 2006.
Zhao, C., Wang, Y., and Zeng, T.: East China plains: a “basin” of ozone pollution, Environ. Sci. Technol., 43, 1911–1915, 2009.
Zhou, D. K., Larar, A. M., Liu, X., Smith, W. L., Strow, L. L., Yang, P., Schlussel, P., and Calbet, X.: Global land surface emissivity retrieved from satellite ultraspectral IR measurements, IEEE T. Geosci. Remote, 49, 1277–1290, 2011.

ACPD
15, 9203–9252, 2015

Table 1. Ozonesonde stations used for the validation. *N* days represents the number of measurements matching the coincidence criteria.

Station	Location		*N* days	Station	Location		*N* days
Ankara	39.97° N	32.86° E	50	Tateno[a]	36.10° N	140.10° E	4
Aquila	42.38° N	13.31° E	11	Uccle	50.80° N	4.35° E	390
Barajas	40.47° N	3.58° W	139	Ushuaia	54.85° S	68.31° W	2
Beijing[a]	39.54° N	117.12° E	7	Valentia	51.93° N	10.25° W	33
Bratts Lake	50.20° N	104.70° W	56	Wallops Island	37.90° N	75.70° W	15
Broadmeadows	37.69° S	144.94° E	19				
Churchill	58.74° N	94.07° W	46	Hanoi	21.02° N	105.80° E	16
De Bilt	52.10° N	5.18° E	104	Hilo	19.43° N	155.04° W	62
Edmonton	53.55° N	114.11° W	2	Hong Kong[a]	22.31° N	114.17° E	93
Egbert	44.23° N	79.78° W	57	Irene	25.90° S	28.22° E	4
Goose Bay	53.31° N	60.36° W	98	Java	7.50° S	112.60° E	6
Hohenpeissenberg	47.80° N	11.00° W	319	Kuala Lumpur	2.73° N	101.70° E	5
Huntsville	34.72° N	86.64° W	9	Nairobi	1.27° S	36.80° E	78
Kelowna	49.93° N	119.40° W	124	Naha[a]	26.20° N	127.70° E	0
Lauder	45.04° S	169.68° E	5	Natal	5.49° S	35.80° W	64
Legionowo	52.40° N	20.97° E	133	Pago	14.23° S	170.56° W	13
Lindenberg	52.21° N	14.12° E	148	Panama	7.75° N	80.25° W	2
Macquarie Island	54.50° S	158.94° E	1	Reunion	21.06° S	55.48° E	87
Payerne	46.49° N	6.57° E	389	Samoa	14.23° S	170.56° W	3
Praha	50.01° N	14.45° E	143	San Cristobal	0.92° S	89.60° W	24
Sapporo[a]	43.10° N	141.30° E	12	Santa Cruz	28.46° N	16.26° W	2
Stony Plain	53.55° N	114.11° W	57	Watukosek	7.50° S	112.60° E	16

[a] The time coincidence criterion is relaxed to 24 h for the validation dedicated to East Asia in order to allow a larger number of coincidence with IASI observations (most of the observations are done in the afternoon). The number of measurements used for each station is: Beijing – 7, Hong Kong – 130, Naha – 147, Sapporo – 193, Tateno – 132.

ACPD
15, 9203–9252, 2015

Table 2. Validation results. The bias (IASI-sonde), the RMS and the correlation coefficient are provided for different partial columns of ozone. LT: Lower tropospheric column from surface to 6 km (a.s.l.), TROPO: tropospheric column from surface to 11 km, UTLS: column from 8 to 16 km, STRATO: column from 16 to 30 km, and TOTAL: column from surface to 30 km. The bias and the RMS are given in DU and in percent in parenthesis.

	Bias	RMS	r
LT	−0.6 (2.8)	2.8 (13.7)	0.70
TROPO	1.8 (4.7)	5.7 (14.6)	0.84
UTLS	8.9 (18.7)	8.6 (18.0)	0.96
STRATO	6.2 (17.9)	6.3 (18.2)	0.95
TOTAL	0.7 (0.3)	16.0 (6.0)	0.95

ACPD
15, 9203–9252, 2015

Figure 1. Geographical domain used for the study.

ACPD
15, 9203–9252, 2015

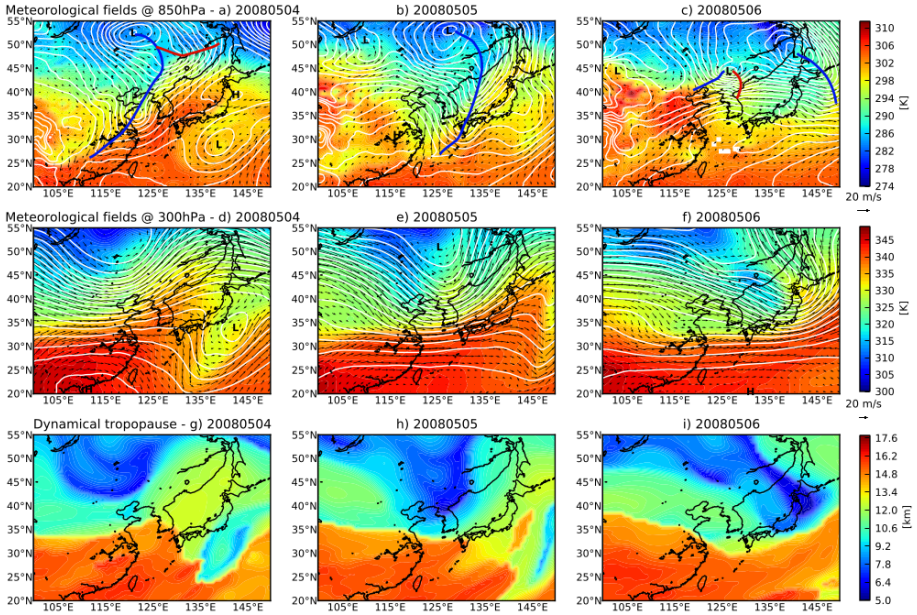

Figure 2. Meteorological situation given at **(a)** 850 hPa and **(b)** 300 hPa from 4 to 6 May 2008 as well as **(c)** the dynamical tropopause. All the meteorological are derived from the ERA-Interim reanalysis. The colored filled contours in **(a)** and **(b)** represent the equivalent potential temperature, and the white contour the geopotential height. The "L" and "H" symbols represent the centre of the lows and highs respectively. The horizontal winds are also plotted. The cold and warm front are displayed in blue and red respectively on the top panel.

ACPD
15, 9203–9252, 2015

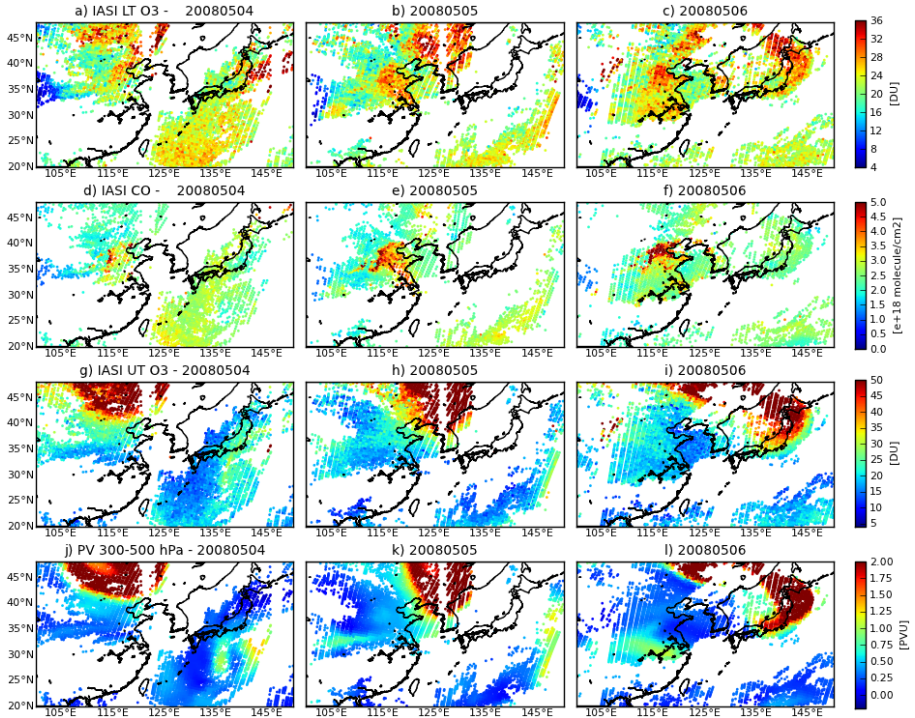

Figure 3. (a) Lower tropospheric ozone columns (surface to 6 km a.s.l.) retrieved from IASI from 4 to 6 May 2008; **(b)** Total CO columns from IASI; **(c)** Upper tropospheric ozone columns (6 to 12 km a.s.l.) retrieved from IASI; **(d)** Potential Vorticity (PV) from ERA-Interim reanalysis averaged between 300 and 500 hPa.

ACPD
15, 9203–9252, 2015

Springtime variability of lower tropospheric ozone

G. Dufour et al.

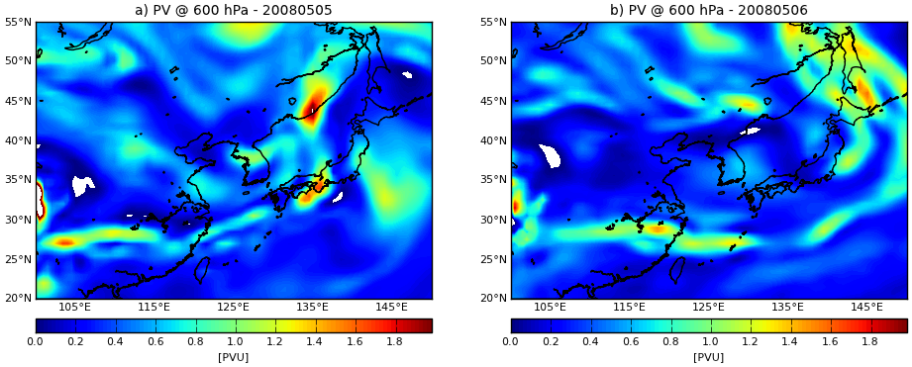

Figure 4. Potential Vorticity (PV) at 600 hPa from ERA-Interim reanalysis on 5 and 6 May 2008.

ACPD
15, 9203–9252, 2015

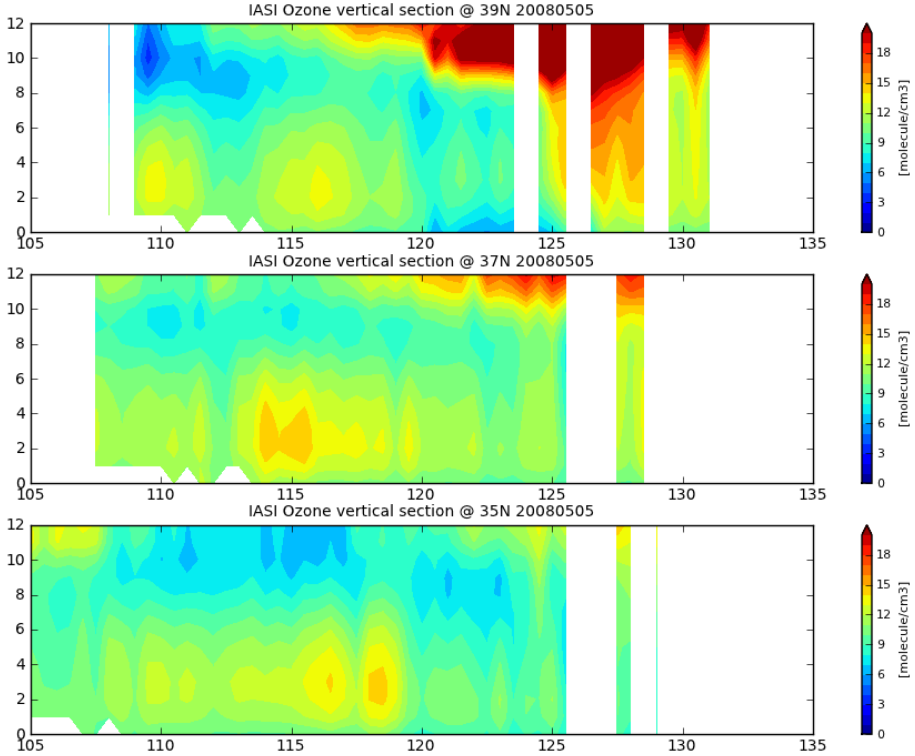

Figure 5. Vertical section of ozone concentration profiles retrieved with IASI against longitude within 1° latitudinal band at 39, 37, and 35° N on 5 May 2008.

ACPD
15, 9203–9252, 2015

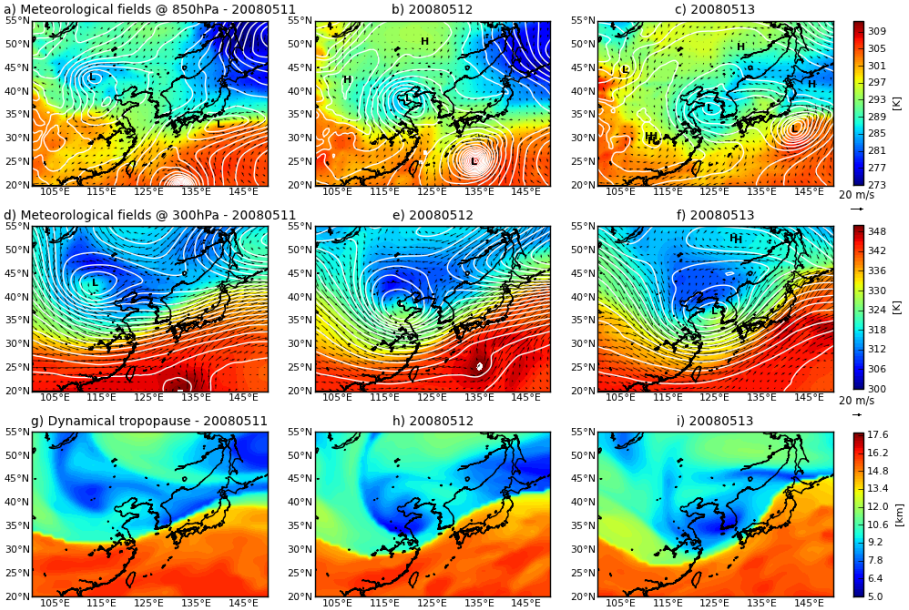

Figure 6. Same as Fig. 2 for 11 to 13 May 2008.

ACPD
15, 9203–9252, 2015

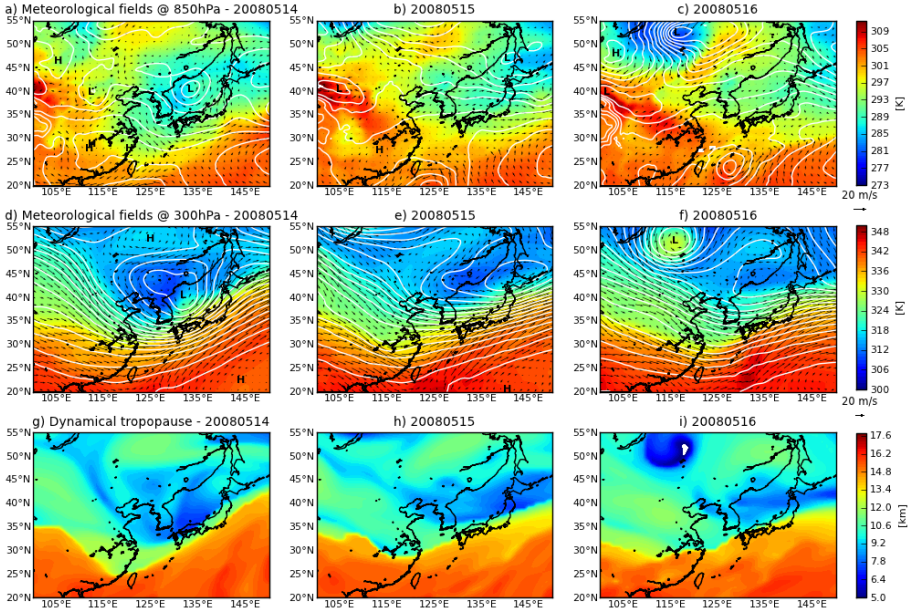

Figure 7. Same as Fig. 2 for 14 to 16 May 2008.

ACPD
15, 9203–9252, 2015

Springtime variability of lower tropospheric ozone

G. Dufour et al.

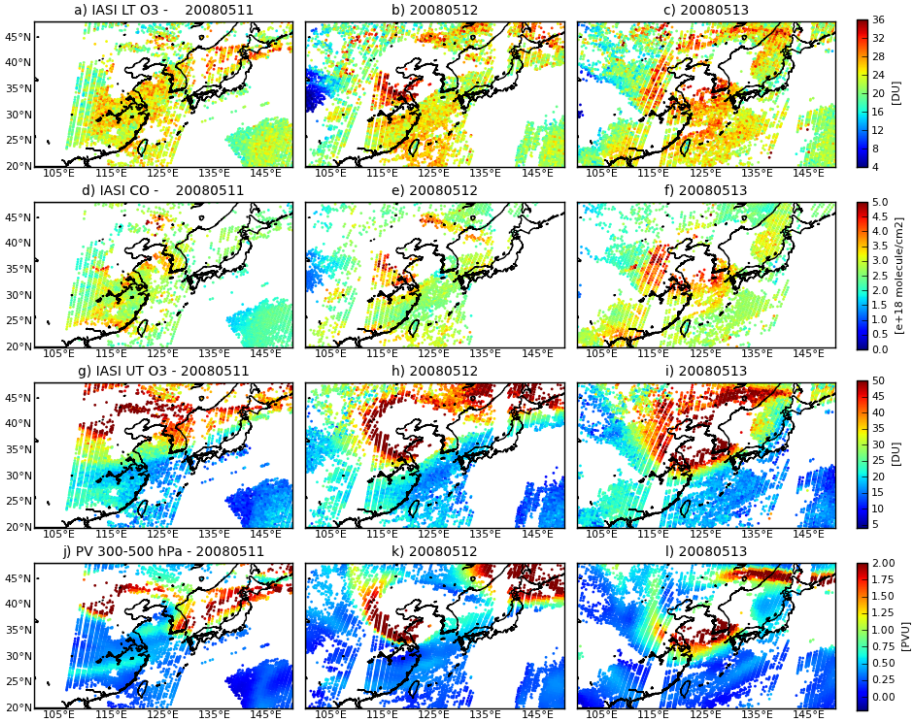

Figure 8. Same as Fig. 3 for the 11–13 May 2008 period.

ACPD
15, 9203–9252, 2015

Springtime variability of lower tropospheric ozone

G. Dufour et al.

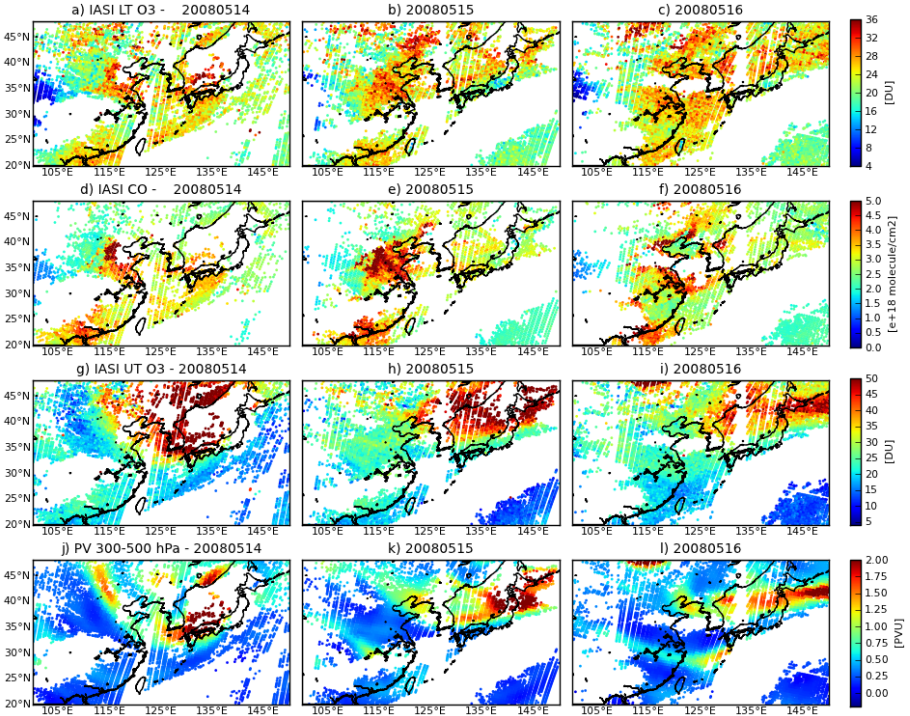

Figure 9. Same as Fig. 3 for the 14–16 May 2008 period.

ACPD
15, 9203–9252, 2015

Springtime variability of lower tropospheric ozone

G. Dufour et al.

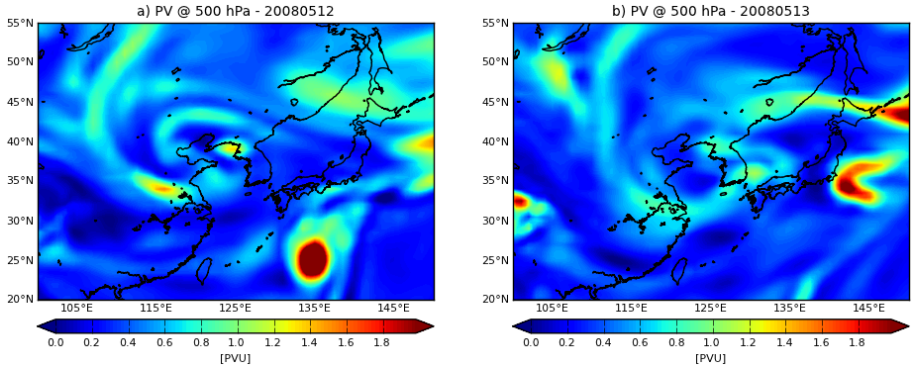

Figure 10. Potential Vorticity (PV) at 500 hPa from ERA-Interim reanalysis on 12 and 13 May 2008.

ACPD
15, 9203–9252, 2015

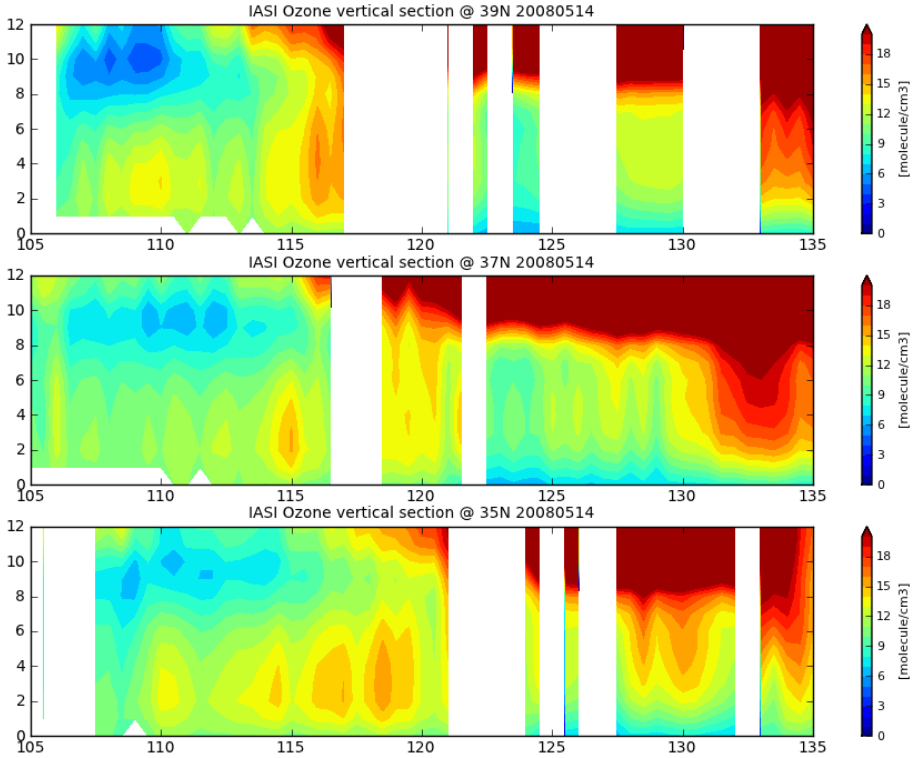

Figure 11. Vertical section of ozone concentration profiles retrieved with IASI against longitude within 1° latitudinal band at 39, 37, and 35° N on 14 May 2008.

ACPD
15, 9203–9252, 2015

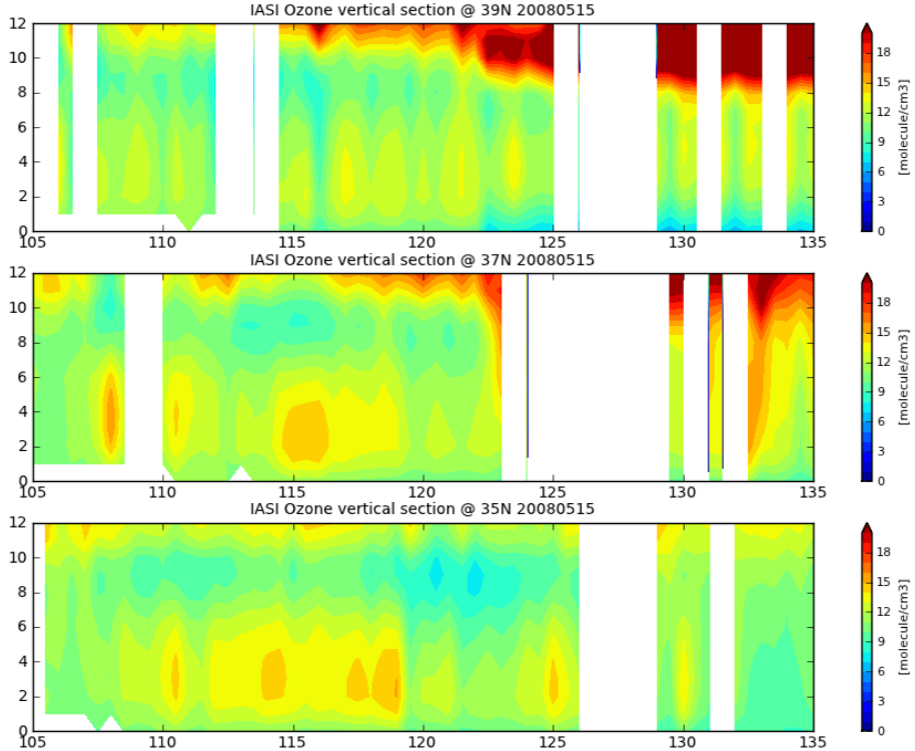

Figure 12. Vertical section of ozone concentration profiles retrieved with IASI against longitude within 1° latitudinal band at 39, 37, and 35° N on 15 May 2008.

ACPD
15, 9203–9252, 2015

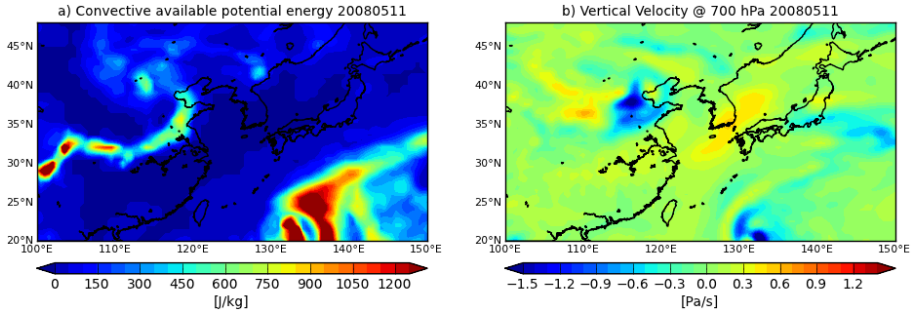

Figure 13. Convective available potential energy **(a)** and vertical velocity at 700 hPa **(b)** from ERA-Interim reanalysis.

ACPD
15, 9203–9252, 2015

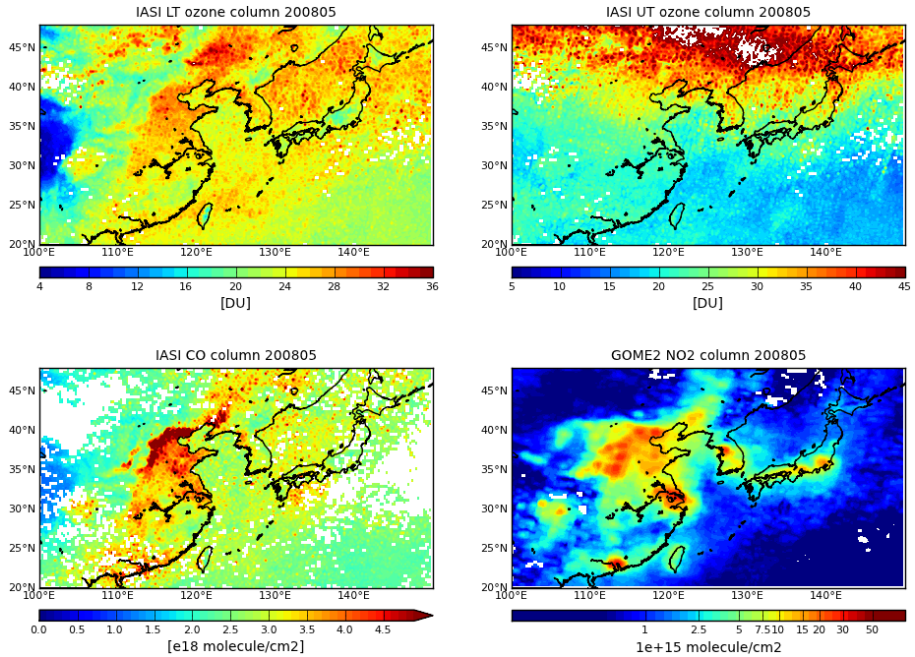

Figure 14. Monthly lower (upper left) and upper (upper right) tropospheric ozone columns observed by IASI in May 2008 as well as monthly IASI total CO columns (lower left) and GOME-2 NO_2 tropospheric columns (lower right) observed in May 2008. The average is calculated for a 0.25° × 0.25° resolution grid.

ACPD
15, 9203–9252, 2015

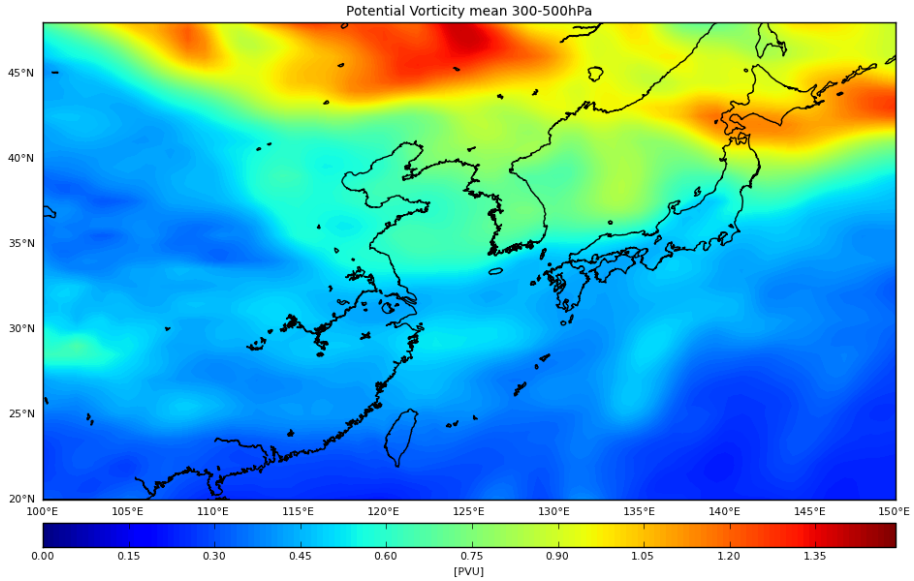

Figure 15. Monthly Potential Vorticity from ERA-Interim reanalysis averaged between 300 and 500 hPa with a horizontal resolution of 0.5°.

ACPD
15, 9203–9252, 2015